

Nonholonomic Virtual Constraints for Dynamic Walking

Brent Griffin and Jessy Grizzle

Abstract—Virtual constraints are functional relations (*i.e.*, *constraints*) on the state variables of a robot’s model that are achieved through the action of actuators and feedback control instead of physical contact forces. They are called *virtual* because they can be re-programmed on the fly without modifying any physical connections among the links of the robot or its environment. Previous analytical and experimental work has established that vector relative degree two virtual *holonomic* (*i.e.*, only configuration dependent) constraints are a powerful means to synchronize the links of a bipedal robot so as to achieve walking and running motions over a variety of terrain profiles. This paper introduces a class of virtual *nonholonomic* constraints that depend on velocity through (generalized) angular momentum, while maintaining the property of being relative degree two. This additional freedom is shown to yield control solutions that handle a wider range of gait perturbations arising from terrain variations and exogenous forces. Moreover, including angular momentum in the virtual constraints allows foot placement control to be rigorously designed on the basis of the full dynamic model of the biped, instead of on the basis of an inverted pendulum approximation of its center of mass, as is commonly done in the bipedal robotics literature. This new class of control laws is shown in simulation to be robust to a variety of common gait disturbances.

I. INTRODUCTION

Virtual *holonomic* constraints are functional relations among the configuration variables of a robot that are dynamically imposed through feedback control. Their purpose is to synchronize the evolution of the various links to an internal *phase or gait timing variable*, such as the position of the robot’s hip with respect to the stance leg end [1]. The gait timing variable is selected to be monotonically increasing along a walking motion so that it can replace time as a means to parameterize command “trajectories”. From a theoretical perspective, virtual constraints turn the Isidori-Byrnes theory of nonlinear zero dynamics [2] into a formal gait and feedback design tool, while the experiments reported in [3]–[8] attest to the applicability of the approach to realize dynamic locomotion that meets a range of design objectives, from speed of locomotion, to limits on actuator torque, and available friction cone, to only name a few.

The purpose of this paper is to introduce a more general class of *nonholonomic* virtual constraints that depend on velocity. The motivation for this extension comes from the work of [9], which plans the desired placement of a biped’s swing foot as a function of the center of mass velocity in the horizontal direction. The control law for foot placement

is based on the linear inverted pendulum model (aka LIP) proposed in [10], which approximates the robot’s dynamics as an inverted pendulum with constant vertical height and massless legs, as shown in Fig. 1. Due to the assumptions of constant vertical height and massless legs, the pendulum’s dynamic model is linear, the reset map associated with leg impact is linear and energy conserving, and the overall hybrid model can be solved in closed form. From the closed-form solution of the LIP model, Pratt et al. [9], [11] propose a foot placement policy to regulate forward walking speed, and have illustrated it on complex robots, such as a simulation model of the M2V2 biped undergoing “shoves” of up to 15 Ns [12].

In this paper, a velocity-dependent foot-placement strategy is designed and implemented without relying on an inverted pendulum approximation of the robot. In particular, the distributed mass, multi-link nature of the robot can be fully taken into account, including energy losses at impacts. The control law is implemented through a set of virtual constraints that depend on velocity through angular momentum about that stance leg end, in addition to the robot’s configuration variables. A set of parameterized splines appearing in the virtual constraints are designed through a parameter optimization process developed in [13], that explicitly allows potential terrain profile variations to be taken into account during the design of a periodic orbit [14]. The robustness of the resulting control law to terrain and velocity perturbations

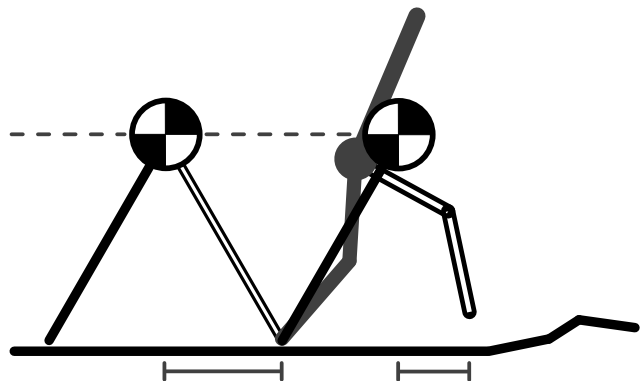


Fig. 1: Velocity-based swing foot placement has been designed on the basis of the linear inverted pendulum model [9]. Using velocity-dependent virtual constraints, it is possible to implement a swing foot placement policy that accounts for the full dynamics of the biped, as well as a range of terrain disturbances.

Brent Griffin and Jessy Grizzle are with the Department of Electrical Engineering and Computer Science, University of Michigan, Ann Arbor, MI 48109 USA e-mail: {griffb, grizzle}@umich.edu.

This work was supported by NSF grants ECCS-1343720 and ECCS-1231171.

is evaluated through simulation and compared to other control laws. The control law based on *nonholonomic constraints* is able to accommodate a wider range of perturbations than a control law based on *holonomic constraints*.

In related work on terrain variations, an event-based controller is given in [15] that updates parameters in a continuous-time controller in order to achieve a *dead-beat control response*, in the sense that following a change in terrain height, in one step it steers the robot's state back to its nominal value on the periodic orbit. A control architecture that *switches among a finite-set of controllers* when dealing with terrain variation is studied in [4], [16]. A time-invariant linear controller is developed in [17] using transverse linearization [18] and a receding-horizon control framework, with experiments performed on a compass-gait walker.

The current paper develops a single (non-switching) controller and nominal periodic gait that are insensitive to a predetermined and finite set of terrain variations and velocity perturbations. This choice of a non-switching controller is motivated in part by ease of implementation, but even in the context of a switching controller, it would be desirable that one of the controllers be insensitive to a pre-determined range of disturbances. Two feedback controllers are studied that use nonholonomic virtual constraints. The first is an application of the *Optimization for Accommodation of Unknown Terrain Disturbances* method presented in [13] applied to nonholonomic constraints. The second is an implementation of swing foot placement [9] with the following improvements:

- foot placement is based on velocity throughout the step and not just the horizontal velocity of the center of mass at mid-step;
- the dynamics of the full model including impact losses and varying center of mass height are included; and
- a pre-specified range of terrain disturbances are included in the controller design process.

With respect to prior work with virtual constraints, the primary contributions include:

- the introduction of a new class of virtual constraints that include angular momentum, but maintain control outputs that are relative degree two for ease of implementation; and
- the demonstration of superior ability to attenuate velocity perturbations.

II. NONHOLONOMIC VIRTUAL CONSTRAINTS

Assume an n -degree of freedom mechanical model

$$D(q)\ddot{q} + C(q, \dot{q})\dot{q} + G(q) = Bu, \quad (1)$$

with Lagrangian

$$\mathcal{L}(q, \dot{q}) := \frac{1}{2}\dot{q}^\top D(q)\dot{q} - V(q). \quad (2)$$

Assume moreover that the configuration variables $q = (q_u, q_a)$ have been selected such that $q_u = (q_1, \dots, q_m)$ are

unactuated and $q_a = (q_{(m+1)}, \dots, q_n)$ are actuated, so that, by Lagrange's equation

$$\frac{d}{dt} \frac{\partial \mathcal{L}}{\partial \dot{q}_u} - \frac{\partial \mathcal{L}}{\partial q_u} = 0. \quad (3)$$

The quantity

$$\sigma := \frac{\partial \mathcal{L}}{\partial \dot{q}_u}(q, \dot{q}) \quad (4)$$

is the *momenta conjugate* to q_u , and for $1 \leq i \leq m$, is equal to

$$\sigma_i = D_i(q)\dot{q}, \quad (5)$$

where $D_i(q)$ is the i th row of the mass-inertia matrix. From (3) and (4),

$$\frac{d}{dt} \sigma = \frac{\partial \mathcal{L}}{\partial q_u}(q, \dot{q}), \quad (6)$$

and thus if σ has a relative degree, is two or greater. Indeed, differentiating σ a second time gives terms that depend on acceleration, which via (1), may in turn depend on the input torque.

Functional relations involving *momenta* are classic examples of *nonholonomic constraints* [19]. Consider now a virtual constraint built from an output function of the form

$$y = h(q, \sigma) \quad (7)$$

$$=: \tilde{h}(q, \dot{q}). \quad (8)$$

Then from the chain rule, its derivative along trajectories of the model is

$$\begin{aligned} \dot{y} &= \frac{\partial h(q, \sigma)}{\partial q} \dot{q} + \frac{\partial h(q, \sigma)}{\partial \sigma} \dot{\sigma} \\ &= \frac{\partial h(q, \sigma)}{\partial q} \dot{q} + \frac{\partial h(q, \sigma)}{\partial \sigma} \frac{\partial \mathcal{L}}{\partial q_u}(q, \dot{q}) \end{aligned} \quad (9)$$

and thus the relative degree cannot be less than two.

Remark: Equation (9) holds for one or more degrees of underactuation. Thus, it can be applied to both planar and 3D biped models, as well as models with or without compliant elements.

III. CONTROL DESIGN

This section details the controller's design using the non-holonomic virtual constraints presented in Section II.

A. Bipedal Robot MARLO

The robot MARLO¹ is shown in Fig. 2 and is described in detail in [21]. The robot's mass is approximately 55 kg and its legs are one meter long. For this study, the robot is attached to a boom, making it planar. Furthermore, while the robot has series elastic actuators, the springs are sufficiently stiff that in this study they are ignored. The resulting model has five DOF in single support and four actuators.

¹This is the Michigan copy of the ATRIAS-series of robots built by Jonathan Hurst [20].

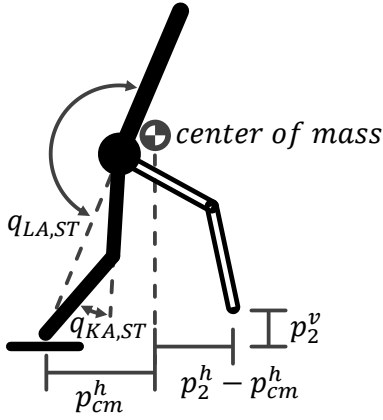
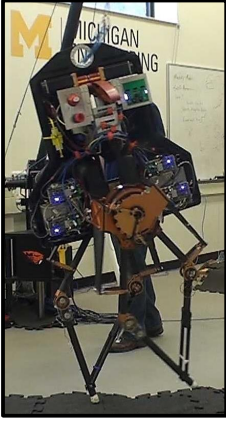


Fig. 2: Robot MARLO and state description for planar model of MARLO used for simulation and control design.

The configuration variables are defined in Fig. 2. Specifically,

$$q_u = p_{cm}^h, \quad (10)$$

where p_{cm}^h is the horizontal position of the center of mass relative to the stance foot and

$$q_a = \begin{bmatrix} q_{LA,ST} \\ q_{KA,ST} \\ p_2^h - p_{cm}^h \\ p_2^v \end{bmatrix}. \quad (11)$$

LA and KA are abbreviations of leg angle and knee angle, ST designates the stance leg, and p_2^h and p_2^v are the horizontal and vertical positions of the swing foot relative to the stance foot. *With this choice of configuration variables, σ is the angular momentum about the stance foot end.*

The complete hybrid model of the robot is derived as in [21], including the dynamic model for the single support phase and the reset map at leg impact. Using the natural state variables $x = (q; \dot{q})$, the Lagrange model (1) is expressed in state variable form as in (29), with $x \in \mathcal{X}$ an open subset of \mathbb{R}^{10} and $u \in \mathbb{R}^4$. The model has one degree of underactuation during single support. For reasons of space, the impact surface (subset of \mathcal{X} corresponding to the height of the swing leg end equaling ground height) and the reset map (new initial condition for the continuous dynamics resulting from the impact) are not discussed here. They are briefly indicated in the appendix; full details are in [21] and [1].

B. Family of Feedback Controllers

The feedback controller is designed using the method of *virtual constraints* and *hybrid zero dynamics* [22], [23]. For planar MARLO, four virtual constraints are defined, one for each available actuator. The output vector y is defined in terms of the configuration variables, q , angular momentum, σ , and a set of parameters κ and β ,

$$y = h(q, \sigma, \kappa, \beta) \quad (12)$$

in such a way that the output has vector relative degree 2 [2, pp. 220] on a subset of interest, $\mathcal{X} \times \mathcal{K} \times \mathcal{B}$. The

parameters κ are used to achieve invariance of the *zero dynamics* manifold induced by (12), while the parameters β will be tuned through optimization to achieve a desirable periodic orbit.

The feedback controller is based on input-output linearization, namely

$$u_{ff}(q, \dot{q}, \kappa, \beta) := -[L_g L_f h(q, \dot{q}, \kappa, \beta)]^{-1} L_f^2 h(q, \dot{q}, \kappa, \beta), \quad (13)$$

$$u_{fb}(q, \dot{q}, \kappa, \beta) := -[L_g L_f h(q, \dot{q}, \kappa, \beta)]^{-1} (K_p y + K_d \dot{y}), \quad (14)$$

with

$$u = \Gamma(q, \dot{q}, \kappa, \beta) := u_{ff}(q, \dot{q}, \kappa, \beta) + u_{fb}(q, \dot{q}, \kappa, \beta). \quad (15)$$

Along solutions of the closed-loop system,

$$\ddot{y} + K_d \dot{y} + K_p y \equiv 0. \quad (16)$$

An explicit choice of $h(q, \sigma, \kappa, \beta)$ is now made,

$$\begin{aligned} h(q, \sigma, \kappa, \beta) &= h_0(q) - h_d(\tau(q), \sigma, \kappa, \beta), \quad (17) \\ &= h_0(q) - [h_{d,\sigma}(\sigma, \beta) + h_{d,\tau}(\tau(q), \kappa, \beta)], \quad (18) \end{aligned}$$

where $h_d(\tau(q), \sigma, \kappa, \beta)$ specifies the desired evolution of $h_0(q)$ and

$$h_0(q) = q_a, \quad (19)$$

$$h_{d,\sigma}(\sigma, \beta) = [0, 0, k_1(\beta)\sigma + k_2(\beta)\sigma^2, 0]'. \quad (20)$$

The inclusion of angular momentum in the third component of $h_{d,\sigma}$ allows step length to vary with velocity. The function $h_{d,\tau}(\tau(q), \kappa, \beta) \in \mathbb{R}^4$ is a vector of splines that specifies desired evolution of defined $h_0(q) - h_{d,\sigma}(\sigma, \beta)$ in terms of the gait phasing variable $\tau(q)$. Here, the splines are Bézier polynomials, with the i th polynomial given by

$$h_{d,\tau,i}(\tau, \kappa, \beta) := \sum_{k=0}^M \alpha_{i,k} \frac{M!}{k!(M-k)!} \tau^k (1-\tau)^{M-k}, \quad (21)$$

where the four degree- M Bézier polynomials are defined by $\alpha(\kappa, \beta) \in \mathbb{R}^{4 \times (M+1)}$ [1, pp. 138]. The gait phasing variable $\tau(q)$ is selected to be an affine function of p_{cm}^h and is normalized on the periodic orbit to take values in $[0, 1]$.

The complete output equation using (12) and (18)-(21) is

$$y = \begin{bmatrix} q_{LA,ST} \\ q_{KA,ST} \\ p_2^h - p_{cm}^h \\ p_2^v \end{bmatrix} - \begin{bmatrix} 0 \\ 0 \\ k_1\sigma + k_2\sigma^2 \\ 0 \end{bmatrix} - h_{d,\tau}(\tau(q), \kappa, \beta). \quad (22)$$

In the optimization phase, values for k_1 and k_2 will be chosen such that a perturbation in velocity, and attendant deviation of σ , results in a corrective change in swing foot placement. Specifically, this will adjust the amount of time the center of mass spends behind the stance foot, versus in front of the stance foot, and will enable quicker convergence to the periodic orbit [9]–[11].

C. Optimization for Three Control Solutions

Three controllers are designed and subsequently tuned via parameter optimization: a controller that does not include nonholonomic virtual constraints and two controllers that do. These will be denoted as HVC, NHVC, and NHVC-SFP, where HVC and NHVC refer to the use of holonomic and nonholonomic virtual constraints, respectively, and SFP refers to an additional objective of swing foot placement suggested by the LIP model. The controller based on HVC serves as a comparison to work in [13]. The swing foot placement policy used for the NHVC-SFP optimization is derived in Section IV.

To account for uneven terrain, the *Optimization for Accommodation of Unknown Terrain Disturbances* method presented in [13] is used. This is a parameter optimization problem in (β, x_0) , the parameters in h_d and the initial state of the robot, such that the resulting closed-loop system has a periodic solution and can also accommodate (i.e., take valid steps following) a given set of terrain disturbances. The cost function is chosen as in [13] and [14] so that it favors perturbed solutions that “return closely” to the nominal periodic solution; in other words, the cost functions is designed so that the closed-loop system attenuates the potentially deleterious effects of the given set of ground height variations. A key feature is that the gait phasing variable is used to penalize more heavily deviations that persist “late” into the gait.

Two primary changes have been made with respect to [13]. First, nonholonomic virtual constraints are incorporated using (20) as the outputs. Second, two steps following a terrain disturbance are included in the cost so that the effect of swing foot placement at the end of the first step after the perturbation is captured during the second step.

Our optimization cost to penalize deviations is induced by 4 terrain height disturbances in $D = \{\pm 4 \text{ cm}, \pm 8 \text{ cm}\}$. The nominal periodic solution corresponds to a terrain height of 0 cm. For perturbed steps $1 \leq j \leq 8$, the deviation costs are defined as

$$\mathcal{J}_j = \frac{1}{(\tau_j^- - \tau_j^+)} \int_{\tau_j^+}^{\tau_j^-} (\|\delta x_j(\tau)\|^2 + \|\delta u_j(\tau)\|^2) \frac{(\tau - \tau_j^+)}{(\tau_j^- - \tau_j^+)} d\tau. \quad (23)$$

$\delta x_j(\tau)$ and $\delta u_j(\tau)$ are the differences in perturbed state and control trajectories from the closest existing periodic trajectories characterized by τ ². The term $\frac{(\tau - \tau_j^+)}{(\tau_j^- - \tau_j^+)}$ under the integral scales the errors so that initial deviations from the nominal periodic trajectory are discounted with respect to errors toward the end of the step. The term $\frac{1}{(\tau_j^- - \tau_j^+)}$ outside the integral is included so that perturbed step costs are normalized w.r.t. the varying ranges of τ_j resulting from higher and lower terrain disturbances.

²See [13, Eqn. (16)-(17)]. A more comprehensive approach for calculating errors of perturbed trajectories is available in [24].

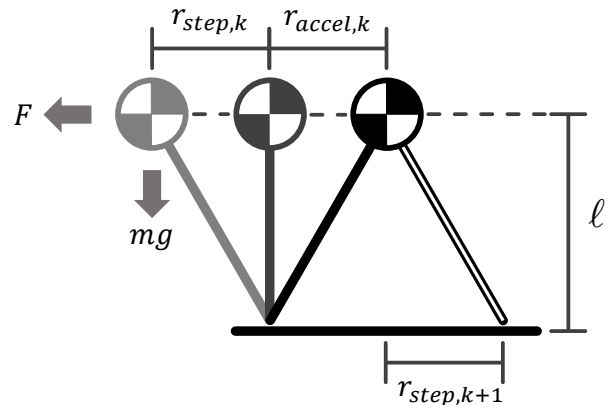


Fig. 3: Linear Inverted Pendulum model. Horizontal force F results from the ground reaction forces caused by gravity.

The overall cost function is

$$\mathcal{J} = \mathcal{J}_0 + \sum_{j=1}^8 w_j \mathcal{J}_j, \quad (24)$$

where w_j determines the relative weight of each perturbation and the energy efficiency \mathcal{J}_0 . \mathcal{J}_0 is calculated using step distance and mechanical actuator work of the nominal solution.

Parameter optimization problem: Find $(\beta; x_0)$ that (locally) minimize \mathcal{J} subject to the existence of a periodic solution that respects the following constraints: motor torque is saturated at 6 Nm; vertical ground reaction force greater than 100 N and friction coefficient less than 0.6; minimum swing foot clearance of 0.1 m over stance foot; minimum knee bend of 10° to avoid hyperextension; average walking speed between 0.6-0.8 m/s. The computations were performed with `fmincon` in MATLAB.

IV. SWING FOOT PLACEMENT USING NONHOLONOMIC VIRTUAL CONSTRAINTS

Figure 3 shows the Linear Inverted Pendulum model used to derive the foot placement strategy of [9]

$$v_{k+1}^2 = v_k^2 - \frac{g}{\ell} (r_{accel,k}^2 - r_{step,k}^2), \quad (25)$$

where k is step number, v_k is the center of mass velocity when the pendulum is vertical, and $r_{step,k}$ and $r_{accel,k}$ are the horizontal distances the center of mass travels from behind the stance foot to in front of the stance foot during step k , resulting in the velocity v_{k+1} in the next step.

For implementation on the full dynamic model of MARLO, adjustments are made to (25). First, the height of the center of mass, ℓ , is calculated in this work as the average center of mass height during the periodic orbit of the full model. Second, (25) does not take impact losses into account and will generally require $r_{accel} > r_{step}$ to compensate for this. Finally, because swing foot height relative to the stance foot is included in (22), r_{accel} does not change when walking on flat ground.

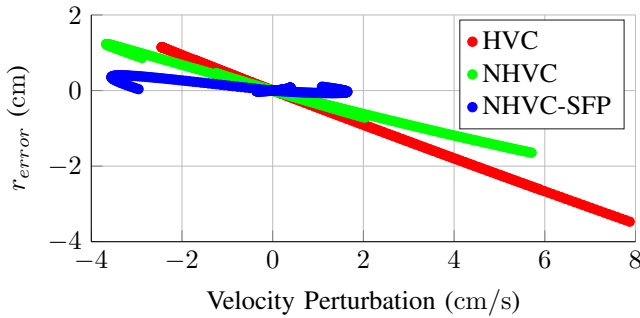


Fig. 4: r_{error} vs. velocity perturbation. Perturbations occur during the two steps following a single terrain height disturbance $d \in [-8, 8]$ (cm).

In (25), let v^* , r_{step}^* , and r_{accel}^* denote nominal values on a periodic orbit, so that

$$v^{*2} = v^2 - \frac{g}{\ell} (r_{accel}^{*2} - r_{step}^{*2}). \quad (26)$$

In (25), setting $r_{accel,k} = r_{accel}^*$ and $v_{k+1} = v^*$ from (26) gives step length to return to the nominal velocity, namely

$$r_{step,k} = \sqrt{\frac{\ell}{g} (v_k^2 - v^{*2}) + r_{step}^{*2}}. \quad (27)$$

The step-length policy (27) is implemented using the full model and nonholonomic virtual constraints. The variable r_{step} is equivalent to the configuration variable $p_2^h - p_{cm}^h$ at the end of a step. Since $p_2^h - p_{cm}^h$ is paired with an angular momentum-based virtual constraint in (22), the horizontal position of the swing foot can vary with velocity.

Define $r_{error,k}$ as the difference between the actual swing foot placement and $r_{step,k}$ from (27). The NHVC-SFP control solution is optimized with an additional cost, \mathcal{J}_{SFP} , based on $r_{error,k}$

$$\mathcal{J} = \mathcal{J}_{SFP} + \mathcal{J}_0 + \sum_{j=1}^8 w_j \mathcal{J}_j. \quad (28)$$

A comparison of the error in r_{step} for the three control solutions is shown in Fig. 4. The NHVC-SFP controller stays within 4 mm of the theoretical swing foot placement policy for the terrain disturbances used during optimization.

V. RESULTS

Simulation results are presented here with discussion given in Section VI. The nominal periodic orbits resulting from the three control solutions are very similar as shown in Table I.

A. Disturbance Types

Figure 5 shows the three types of disturbances used to evaluate each of the control solutions. Step changes in terrain height consist of a vertical displacement of d (m) per step, as was done during optimization. A change in terrain slope of θ (deg) causes a similar disturbance as a step change in terrain height, but accounts for variations in terrain elevation with longer and shorter steps. A sloped terrain may be more

TABLE I: Periodic step velocity, impact losses, and energy efficiency on flat ground.

Metric	Control		
	HVC	NHVC	NHVC-SFP
Step Velocity (m/s)	0.63	0.65	0.66
Impact Losses (J)	19.9	20.1	19.6
Energy Efficiency (J/m) ^a	347	346	365

^aEfficiency is calculated using \mathcal{J}_0 from (24) and (28).

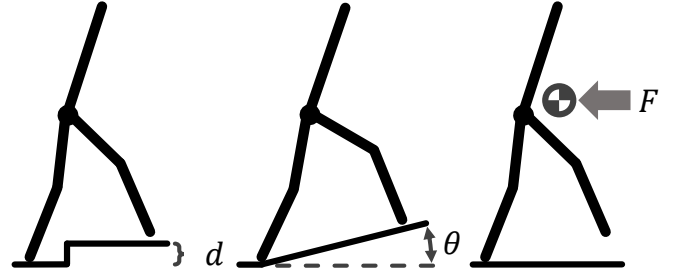


Fig. 5: Step terrain disturbance (left), change in terrain slope (middle), and horizontal force to center of mass (right).

representative of natural outdoor terrain. A third type of disturbance is a horizontal force F (N) applied to the center of mass over the entire duration of a step. This induces a velocity perturbation to the robot without the complication of early or late impacts that may occur with terrain disturbances.

B. Repeated Disturbance Limits

The three control solutions are first compared under the action of a persistent disturbance whose magnitude is gradually increased each step until the robot falls³. For example, with step changes in terrain, each controller is initialized on the periodic orbit, and then the terrain height change is varied as $d_{k+1} = d_k + 0.5$ mm, where k is step number. Once a fall occurs, the simulation is reset from the periodic orbit, and a decrease of 0.5 mm is applied to d_k until failure. The same procedure is applied to terrain slopes with 0.1° increments and to horizontal force with 0.1 N increments. The results of these simulations are summarized in Table II and the resulting perturbed velocities for each step are plotted in Fig. 6.

C. Velocity Perturbation

An additional simulation is performed to evaluate the response of each controller to a velocity perturbation. The velocity perturbation is applied through a ± 25 N horizontal force acting throughout an entire step, starting from the periodic orbit. The response is monitored through the resulting average velocity over the steps following the perturbation. Figure 7 shows the results.

VI. DISCUSSION

While Table I showed that the nominal periodic gait for each controller was similar, differences emerge when testing

³A fall can occur from losing momentum and tumbling backward, or violating ground contact constraints.

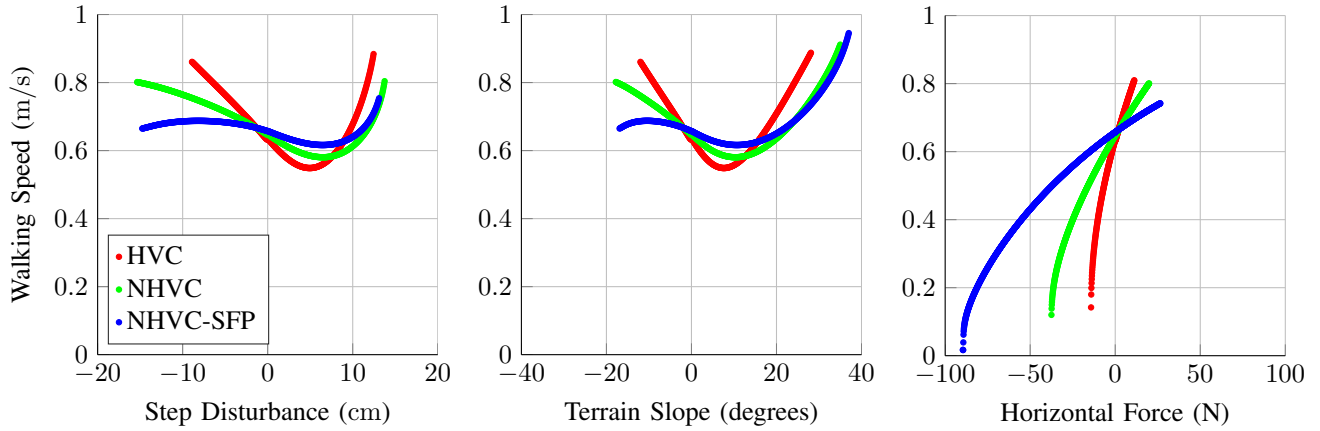


Fig. 6: Velocity vs. step terrain disturbances (left), changes in terrain slope (middle), and external forces on flat ground (right).

TABLE II: Simulation results for all control solutions.

Control	Step Disturbance (cm)			Terrain Slope (degrees)			Horizontal Force (N)		
	Min.	Max.	Rng.	Min.	Max.	Rng.	Min.	Max.	Rng.
HVC	-8.9	12.5	21.4	-12.0	28.1	40.1	-14.2	11.2	25.4
NHVC	-15.4	12.8	28.2	-17.8	35.0	52.8	-37.5	19.9	57.4
NHVC-SFP	-14.8	13.1	27.9	-16.9	37.0	53.9	-89.6	26.5	116.1

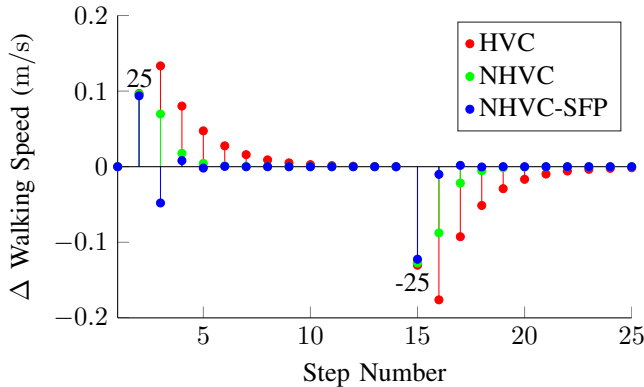


Fig. 7: Velocity stabilization after a 25 N horizontal force applied over entire second step and a -25 N force applied over the entire fifteenth step.

the limits of performance as seen in Table II and Fig. 6. The two controllers using nonholonomic constraints have a similar range on uneven terrain, but both outperform the controller based on holonomic constraints. For all three controllers, velocity initially decreases as expected on uphill disturbances, but then increases as the height change exceeds the limits used in the optimization. The speed up occurs because limited swing foot clearance leads to an early impact, which in turn results in the center of mass initializing the step in a more vertical position; this limits the deceleration period and causes an increase in velocity⁴.

⁴Eventually the speed increases to a point where ground reaction forces are violated.

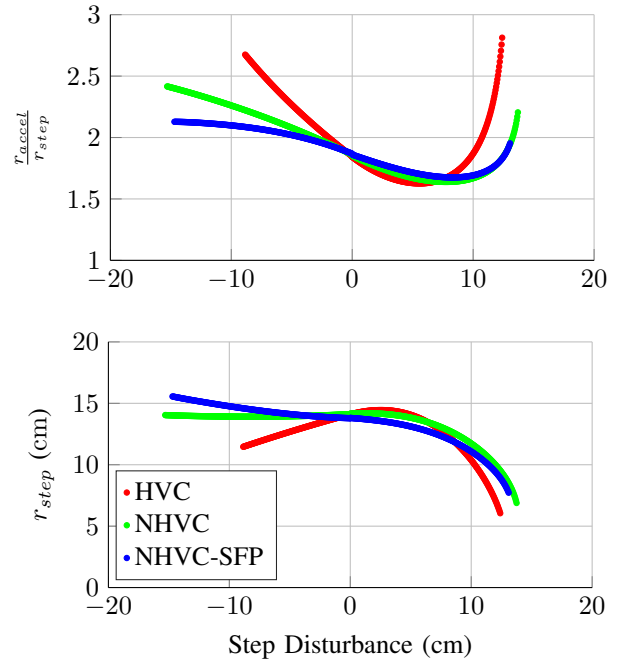


Fig. 8: $\frac{r_{accel}}{r_{step}}$ ratio (top) and r_{step} (bottom) vs. step terrain disturbances.

Figure 8 shows this effect to be most prominent for HVC as r_{step} values, the distance the center of mass must travel to be over the stance foot, are cut nearly in half when moving from 8 cm to 12 cm disturbances. The two controllers using nonholonomic constraints exhibit less variation because r_{step} naturally increases as velocity increases. r_{accel} is consistent between control solutions, increases with downhill walking due to late impacts, and is nominally greater than r_{step} to offset impact losses. NHVC-SFP has the greatest increase in r_{step} for negative disturbances, which leads to tighter velocity regulation in Fig. 6 when walking downhill.

When testing the three control solutions for external forces, the NHVC-SFP controller was able to outperform

the two other controllers by a fair margin, especially for negative horizontal forces. In fact, the NHVC-SFP controller can maintain a periodic gait despite negative impulses as high as 180 Ns per step. Additionally, in Fig. 7 the NHVC-SFP controller exhibits nearly dead-beat behavior for velocity regulation following external forces.

The swing foot placement policy (25) is designed to reject velocity changes when walking on flat ground, and by “embedding this event-based controller” into the NHVC-SFP control solution, the resulting continuous-time swing foot placement policy is able to accommodate a wide range of disturbances. This is especially evident when the external disturbance corresponds to an extreme loss in velocity and changing r_{step} can reduce deceleration from gravity.

VII. CONCLUSIONS

A speed control law suggested by the linear inverted pendulum [9] was embedded into the controller for a planar biped, while accounting for the full ten-dimensional hybrid model of the robot, and also accounting for unexpected terrain height changes. A key factor in the controller design was the use of nonholonomic virtual constraints. Leveraging knowledge from low-dimensional models, as illustrated with swing foot placement, the optimization process was guided toward more successful outcomes. We plan to test this new control policy in the laboratory. Previous work has shown very good agreement between our simulator and planar experiments with MARLO. Additionally, we plan to extend this work to 3D walking to enhance sagittal and frontal plane stability.

APPENDIX I WALKING MODEL

The following material is taken almost verbatim from Sections II and IV of [13]. It is included for the convenience of the reviewers and can be removed before final publication.

A. Hybrid Model

The walking model assumes alternating phases of single support (one foot on the ground) and double support (both feet in contact with the ground). The single support phase assumes the stance foot is not slipping and evolves as a passive pivot. (1) gives a second order model that is expressed in state variable form

$$\dot{x} = f(x) + g(x)u, \quad (29)$$

where $x \in \mathcal{X}$ is the state of the system and $u \in R^{m-n}$ are the control inputs. A parameterized family of continuous-time feedbacks is assumed to be given

$$u = \Gamma(x, \beta), \quad (30)$$

where $\beta \in \mathcal{B}$ are control parameters from an admissible set. The resulting closed-loop system is

$$\dot{x} = f^{cl}(x, \beta) := f(x) + g(x)\Gamma(x, \beta). \quad (31)$$

Local existence and uniqueness of solutions is guaranteed assuming the closed-loop system is continuously differentiable in x and β .

Using the configuration variables from (11), the double support phase occurs when the swing foot strikes the ground which is modeled as

$$p_2^v(x) - d = 0, \quad (32)$$

for $d \in D$, a finite collection of ground heights used to account for varying terrain. It will be assumed at impact that the transversality condition $\dot{p}_2^v(x) < 0$ is met. Physically, this corresponds to the impact occurring at a point in the gait where the swing foot is moving down toward the ground, as opposed to the impact occurring early in the gait which would lead to tripping [4]. The impact is modeled as a collision of rigid bodies using the model of [25]. Consequently, the impact is instantaneous and gives rise to a continuously-differentiable reset map

$$x^+ = \Delta(x^-), \quad (33)$$

that does not depend on the ground height since the vector of pre-impact states, x^- , provides foot height at impact. Here, x^+ is a vector of the post-impact states. As in [1, pp. 57], the impact map is assumed to include leg swapping so that only one continuous-phase mechanical model is needed. Moreover, for reasons that will become clear in Appendix I-B, the impact map is allowed to depend on β .

The overall hybrid model is written as

$$\Sigma : \begin{cases} \dot{x} = f^{cl}(x, \beta) & x^- \notin \mathcal{S}^d \\ x^+ = \Delta(x^-, \beta) & x^- \in \mathcal{S}^d \end{cases} \quad (34)$$

where

$$d \in D := \{d_0, d_1, \dots, d_N\} \quad (35)$$

is the set of ground height variations and

$$\mathcal{S}^d := \{x \in \mathcal{X} \mid p_2^v(x) - d = 0, \dot{p}_2^v(x) < 0\} \quad (36)$$

is the hypersurface in the state space where the swing leg impact occurs at ground height $d \in D$.

Remark: The reference [1, pp. 109] shows how to augment the state variables with control parameters in order to accommodate event-based control, as used in [15]. This extension is employed later in (40).

Model Solutions: For a given value of $\beta \in \mathcal{B}$, a solution of the hybrid model (34) is defined by piecing together solutions of the differential equation (31) and the reset map (33); see [1, pp. 56], [25]. Because we are interested in periodic orbits and their perturbations, we exclude Zeno and other complex behavior from our notion of a solution.

B. Extended Model for Invariant Hybrid Zero Dynamics

Parameters κ are used to maintain *hybrid zero dynamics* following impact deviations. With output (22), it is straightforward to construct a function $\Psi : \mathcal{S}^d \times \mathcal{B} \rightarrow \mathcal{K}$ such that for all

$$\beta \in \mathcal{B} \quad \text{and} \quad \begin{bmatrix} q^+ \\ \dot{q}^+ \end{bmatrix} = \Delta(q^-, \dot{q}^-)$$

the initial values of the outputs are zeroed, that is,

$$\begin{bmatrix} 0 \\ 0 \end{bmatrix} = \begin{bmatrix} y^+ \\ \dot{y}^+ \end{bmatrix} = \begin{bmatrix} h(q^+, \sigma^+, \kappa^+, \beta) \\ \frac{\partial}{\partial q} h(q^+, \sigma^+, \kappa^+, \beta) \dot{q}^+ + \frac{\partial}{\partial \sigma} h(q^+, \sigma^+, \kappa^+, \beta) \dot{\sigma}^+ \end{bmatrix} \quad (37)$$

for $\kappa^+ = \Psi(q^-, \dot{q}^-, \beta)$.

Parameters κ are constant within each step and are reset at the end of each step, hence, they are included as states in the dynamics with

$$x_e := [q, \dot{q}, \kappa]^\top \quad (38)$$

and $\dot{\kappa} = 0$. The extended closed-loop model used is then

$$\Sigma : \begin{cases} \dot{x}_e = f^{cl}(x_e, \beta) & x_e^- \notin \mathcal{S}_e^d \\ x_e^+ = \Delta_e(x_e^-) & x_e^- \in \mathcal{S}_e^d, \end{cases} \quad (39)$$

where

$$f^{cl}(x_e, \beta) = f^{cl}(x, \kappa, \beta) := \begin{bmatrix} f(x) + g(x)\Gamma(x, \kappa, \beta) \\ 0 \end{bmatrix}, \quad (40)$$

$$\Delta_e(x_e^-, \beta) := \begin{bmatrix} \Delta(q^-, \dot{q}^-) \\ \Psi(q^-, \dot{q}^-, \beta) \end{bmatrix}, \quad (41)$$

and

$$\mathcal{S}_e^d := \mathcal{S}^d \times \mathcal{K}. \quad (42)$$

Remarks: (a) (37) is independent of the current value of κ . (b) Because of the second-order system (16) and the reset map in (37), solutions of (40) that are initialized in \mathcal{S}_e^d satisfy $y(t) \equiv 0$. This has two consequences: (i) The solutions evolve on the zero dynamics manifold. (ii) The feedback term u_{fb} in (14) is identically zero, and thus Γ in (15) is independent of the gains K_p and K_d .

ACKNOWLEDGMENT

Hamed Razavi is sincerely thanked for discussions on inverted-pendulum models.

REFERENCES

- [1] E. R. Westervelt, J. W. Grizzle, C. Chevallereau, J. Choi, and B. Morris, *Feedback Control of Dynamic Bipedal Robot Locomotion*, ser. Control and Automation. Boca Raton, FL: CRC Press, June 2007.
- [2] A. Isidori, *Nonlinear Control Systems*, 3rd ed. Berlin: Springer-Verlag, 1995.
- [3] E. R. Westervelt, G. Buche, and J. W. Grizzle, "Experimental validation of a framework for the design of controllers that induce stable walking in planar bipeds," *International Journal of Robotics Research*, vol. 24, no. 6, pp. 559–582, June 2004.
- [4] H. Park, A. Ramezani, and J. W. Grizzle, "A finite-state machine for accommodating unexpected large ground height variations in bipedal robot walking," *IEEE Transactions on Robotics*, vol. 29, no. 29, pp. 331–345, 2013.
- [5] B. G. Buss, A. Ramezani, K. Akbari Hamed, B. A. Griffin, K. S. Galloway, and J. W. Grizzle, "Preliminary walking experiments with underactuated 3d bipedal robot marlo," in *Intelligent Robots and Systems (IROS 2014), 2014 IEEE/RSJ International Conference on*. IEEE, 2014, pp. 2529–2536.
- [6] H. Zhao, W. Ma, A. Ames, and M. Zeagler, "Human-inspired multi-contact locomotion with AMBER2," in *Cyber-Physical Systems (ICCPs), 2014 ACM/IEEE International Conference on*, 2014, pp. 199–210.
- [7] A. E. Martin, D. C. Post, and J. P. Schmedeler, "The effects of foot geometric properties on the gait of planar bipeds walking under HZD-based control," *The International Journal of Robotics Research*, vol. 33, no. 12, pp. 1530–1543, 2014.
- [8] R. D. Gregg, T. Lenzi, L. J. Hargrove, and J. W. Sensinger, "Virtual constraint control of a powered prosthetic leg: From simulation to experiments with transfemoral amputees," *IEEE Transactions on Robotics*, 2014.
- [9] J. Pratt and R. Tedrake, "Velocity-based stability margins for fast bipedal walking," in *Fast Motions in Biomechanics and Robotics*, ser. Lecture Notes in Control and Information Sciences, M. Diehl and K. Mombaur, Eds. Springer Berlin Heidelberg, 2006, vol. 340, pp. 299–324.
- [10] S. Kajita, T. Yamamura, and A. Kobayashi, "Dynamic walking control of biped robot along a potential energy conserving orbit," *IEEE Transactions on Robotics and Automation*, vol. 8, no. 4, pp. 431–37, Aug. 1992.
- [11] T. Koolen, T. de Boer, J. Rebula, A. Goswami, and J. Pratt, "Capturability-based analysis and control of legged locomotion, Part 1: Theory and application to three simple gait models," *The International Journal of Robotics Research*, no. 9, pp. 1094–1113, July.
- [12] J. Pratt, T. Koolen, T. de Boer, J. Rebula, S. Cotton, J. Carff, M. Johnson, and P. Neuhaus, "Capturability-based analysis and control of legged locomotion, Part 2: Application to M2V2, a lower-body humanoid," *The International Journal of Robotics Research*, no. 10, pp. 1117–1133, Aug.
- [13] B. A. Griffin and J. W. Grizzle, "Walking gait optimization for accommodation of unknown terrain height variations," in *American Control Conference*, July 2015.
- [14] H. Dai and R. Tedrake, "Optimizing robust limit cycles for legged locomotion on unknown terrain," in *Decision and Control (CDC), 2012 IEEE 51st Annual Conference on*, 2012, pp. 1207–1213.
- [15] S. Kolathaya and A. D. Ames, "Achieving bipedal locomotion on rough terrain through human-inspired control," in *Safety, Security, and Rescue Robotics (SSRR), 2012 IEEE International Symposium on*. IEEE, 2012, pp. 1–6.
- [16] T. Yang, E. Westervelt, A. Serrani, and J. P. Schmedeler, "A framework for the control of stable aperiodic walking in underactuated planar bipeds," *Autonomous Robots*, vol. 27, no. 3, pp. 277–290, 2009.
- [17] I. R. Manchester, U. Mettin, F. Iida, and R. Tedrake, "Stable dynamic walking over uneven terrain," *The International Journal of Robotics Research*, pp. 265–279, 2011.
- [18] A. S. Shiriaev, L. B. Freidovich, and S. V. Gusev, "Transverse linearization for controlled mechanical systems with several passive degrees of freedom," *Automatic Control, IEEE Transactions on*, vol. 55, no. 4, pp. 893–906, 2010.
- [19] A. M. Bloch, *Nonholonomic Mechanics and Control*. Springer-Verlag, 2003.
- [20] J. Grimes and J. Hurst, "The design of ATRIAS 1.0 a unique monopod, hopping robot," *Climbing and walking Robots and the Support Technologies for Mobile Machines, International Conference on*, 2012.
- [21] A. Ramezani, J. W. Hurst, K. Akbari Hamed, and J. W. Grizzle, "Performance Analysis and Feedback Control of ATRIAS, A Three-Dimensional Bipedal Robot," *Journal of Dynamic Systems, Measurement, and Control*, vol. 136, no. 2, 2014.
- [22] J. W. Grizzle, G. Abba, and F. Plestan, "Asymptotically stable walking for biped robots: Analysis via systems with impulse effects," *IEEE Transactions on Automatic Control*, vol. 46, pp. 51–64, January 2001.
- [23] E. R. Westervelt, J. W. Grizzle, and D. E. Koditschek, "Hybrid zero dynamics of planar biped walkers," *IEEE Transactions on Automatic Control*, vol. 48, no. 1, pp. 42–56, Jan. 2003.
- [24] A. Saccon, N. van de Wouw, and H. Nijmeijer, "Sensitivity analysis of hybrid systems with state jumps with application to trajectory tracking," in *Decision and Control (CDC), 2014 IEEE 53rd Annual Conference on*, Dec 2014, pp. 3065–3070.
- [25] Y. Hürmüzli and D. B. Marghitu, "Rigid body collisions of planar kinematic chains with multiple contact points," *International Journal of Robotics Research*, vol. 13, no. 1, pp. 82–92, 1994.